On the calibration strategy of medium format cameras for direct georeferencing[1]

Derek Lichti, Jan Skaloud*, Philipp Schaer*

Curtin University of Technology, Perth, Australia
*École Polytechnique Fédérale de Lausanne (EPFL), Switzerland

Abstract
This paper presents an all-airborne approach for the geometric self-calibration of medium format digital cameras used in direct georeferencing. The motivation for this research was the problems of variation of distortion within the photographic field and high parameter correlations that can result from laboratory self-calibration. Determination of the lens distortion coefficients requires convergent imaging geometry and this is the primary reason why laboratory calibration is normally preferred. We propose an airborne approach that combines the advantages of strong network geometry with the benefit of external data input. Results from a series of simulations demonstrate the capabilities of this approach in terms of interior orientation parameter precision and parameter de-correlation. Experimental results show promising results, especially in terms of the radial lens distortion coefficients.

Introduction
The geometric calibration of digital cameras used for direct georeferencing (DR) systems is typically performed by self-calibration in a laboratory where the environment is well-controlled and a dedicated array of signalised targets is available (Kremer, 2006; Mostafa, 2003). Thanks to the continuing development of solid state imaging technology, cameras with larger-area sensors (a Hasselblad H2, 22 mega pixel camera is studied here) are commercially available for use in DR systems. Accordingly, this has permitted the use of longer focal length lenses (35 mm in this study, typically even longer, e.g. $\geq$ 50 mm) that can exhibit distortions on the order of several hundreds of micrometres at the extents of the image format, which gives rise to at least two series issues concerning the use of laboratory calibration.

The first is the variation of radial lens distortion as a function of object distance within the photographic field. When the focal length is much smaller than the object distance, the variation within the photographic field is negligible (Fraser, 1997). The effect can be quite significant, though, for longer focal length lenses used at close range, as is the case for laboratory calibration. If uncorrected, this effect can bias the estimated lens distortion coefficients and, ultimately, object points determined via DR. Though the correction model to account for this variation is well-known (Brown, 1971), its application is likely less widespread since it is not accounted for in all self-calibration software packages. Furthermore, this model has been shown to be inadequate when the distortion gradient is large (Fraser and Shortis, 1992). Empirical methods for modelling the variation have been investigated but they are very labour intensive (Fraser and Shortis, 1992; Shortis et al, 1998) as many calibrations must be performed.

The second concern in the lab calibration solution is the correlation between the exterior orientation elements and the interior orientation, particularly the principal distance (PD). In practice the laboratory room dimensions constrain the "depth" of the target field that can be used, which ultimately influences the accuracy of the PD estimation (Luhmann et al, 2006). This is of particular concern for the aforementioned long focal length lenses. Biases to the

[1] International Calibration and Orientation Workshop EuroCOW 2008, Castelldefels, Spain, 30.1-1.2. 2008

interior orientation due to the correlation mechanisms can be tolerated in "conventional" photogrammetry thanks to projective compensation, but not in DR where the bundle adjustment that facilitates the compensation is not performed.

These two factors motivated an investigation into whether aerial self-calibration—for which the variation of distortion throughout the photographic field is truly not an issue—would be a feasible alternative to lab self-calibration of a digital camera used for helicopter-borne DR. A number of simulation studies have been conducted to determine the optimal network geometry that incorporates external data sources: GPS observations of both the camera position and ground control. The inclusion of laser range measurements in the self-calibration was also investigated. Results from these will show that the exterior and interior orientation elements can be de-correlated from the lens distortion parameters to a greater degree than can be realised in a laboratory calibration, providing the flight setup incorporate adequate geometrical design. Finally, the simulations findings are supported by experimental results.

System Description

The DR system studied in this paper is the Scan2map/Helimap system developed at the EPFL (Skaloud et al., 2006). It integrates high accuracy navigation sensors (GPS-L1L2/GLONAS receiver and tactical grade IMU) with medium-range Airborne Laser Scanner (Riegl LMS-Q240-60i) and high-resolution CCD digital (Hasselblad H2, 22 mega pixel) camera. The system is operated from the side of a helicopter and its unconventional design offers several conceptual advantages in comparison with other systems: quick installation (minutes), no need of recalibration after installation, possibility to map vertical or horizontal features with an optimal geometry and maintaining optimal flying parameters for camera and laser sensors at the same time. The products are high-resolution (<1m²) / high precision (~0.1m) DSM/DTM and ortho-rectified image (<0.05m/pixel).

Laboratory Self-Calibration

For the laboratory calibration of the camera, a network of images of the ETH Zurich target field was acquired. The target field used comprised 36 points having an approximate volume of 3.4 m x 2.0 m x 1.1 m. The sixteen images were captured in a convergent configuration (convergence angle of ≈70°) with three also having kappa rotation angles of 90°. Image target centre measurements were conducted using BAAP software developed at ETHZ (Akca, 2006) as well as at EPFL (Schaer, 2006). The subsequent free-network, self-calibrating bundle adjustment was performed by using the BAAP software, as well as Bingo software (Kruck, 2001) but mainly the software developed by the first author (Lichti and Chapman, 1997).

An extensive model identification process was performed in order to ascertain exactly which additional parameters (APs) from the standard physical model (e.g. Fraser, 1997) should be incorporated in the extended collinearity model. It was found through both statistical and graphical analyses that only the principal point (PP), PD and first two terms of radial lens distortion, k_1 and k_2, were necessary. The quantities examined included: the ratio of APs to their estimated standard deviations, correlation coefficients, the reduction in the RMS of residuals gained by adding APs as well as 1D and 2D plots of residuals. Figure 1 shows the radial lens distortion curve, which exhibits considerable distortion (nearly 700 μm) near the maximum radial distance measured of 26 mm.

At this point it is worth highlighting several high parameter correlations as a prelude to the analyses of the aerial self-calibration simulations summarized in the last column of Table 3. First, the maximum correlation (in terms of absolute value) between the PD and the

perspective centre (PC) co-ordinates was 0.84. Second, the maximum correlation between the PP and orientation angles was 0.80, which is caused by well-known functional relationships (Kenefick et al, 1972). The third is the correlation of -0.90 between k_1 and k_2, which is expected. Some noteworthy low correlations that will be discussed later include k_1 and the PC co-ordinates (0.19 maximum absolute value), k_1 and the PD (-0.33) and the k_2 and the PD (0.39).

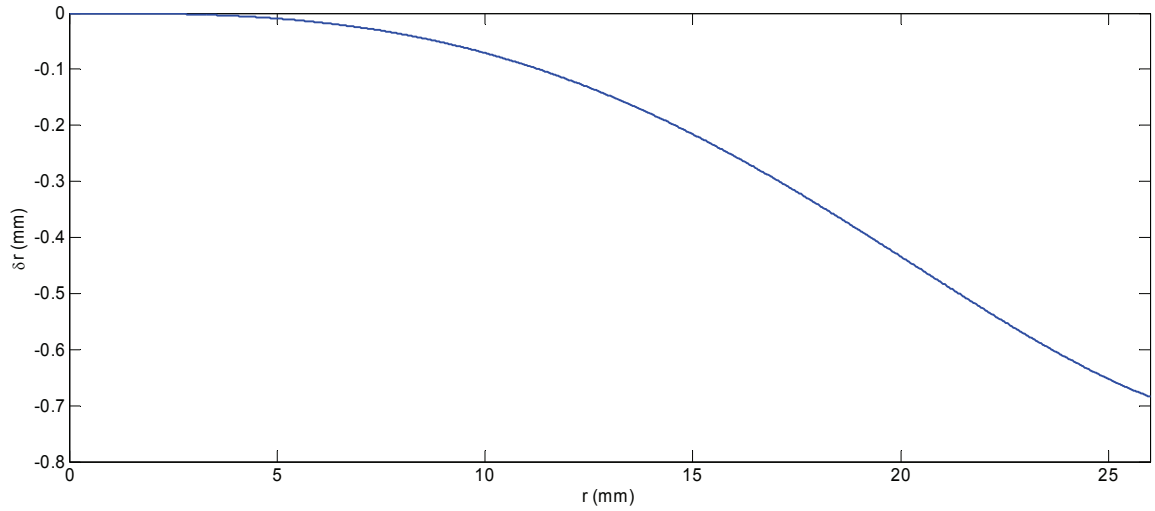

Figure 1. Estimated radial lens distortion profile (δr) from laboratory self-calibration.

Variation of Radial Lens Distortion within the Photographic Field

The model proposed by Brown (1971) was used to calculate the effect of variation within the photographic field for the lens in question. The focus distance of the lens was set to infinity for the lab calibrations and images were acquired at nominal object distances of 2.0 m and 4.0 m. Figure 2 shows the differences between the distortion profiles at the two lab calibration object distances (s′) and the profile at infinite object distance. Clearly the differences are significant: up to 9 μm for the 2.0 m object distance at radial distance of about 20 mm, very close to the inflection point of the estimated distortion curve. The significance can be judged in terms of either the RMS of the laboratory self-calibration image point residuals, which was 0.4 μm, or the propagated uncertainty of the two-term (k_1 and k_2) distortion profile at r=26 mm which was 0.7 um at 68% confidence.

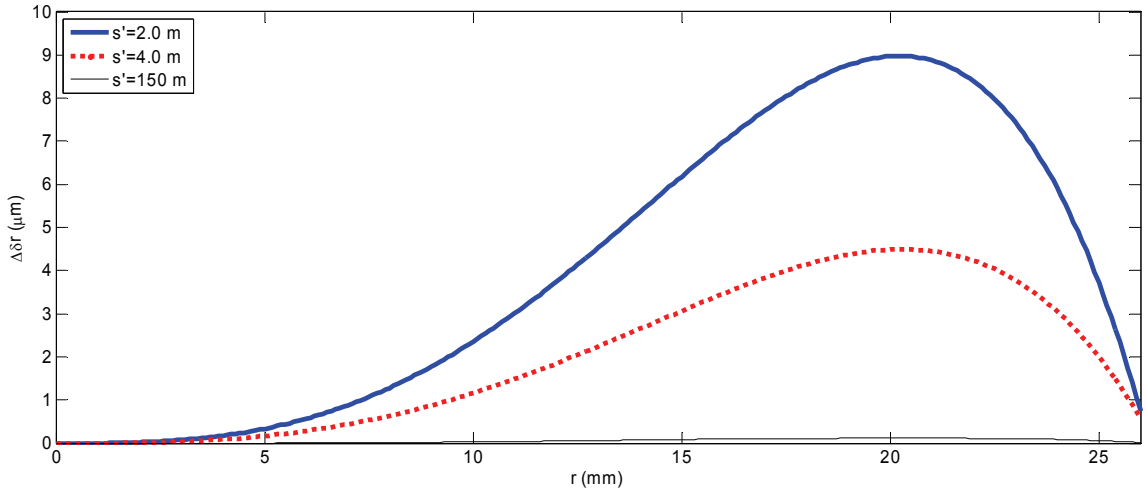

Figure 2. Differences in radial lens distortion profiles (Δδr) due to variation within the photographic field according to Brown's (1971) formula for three object distances, s′.

Though admittedly the known shortcomings of Brown's model have been neglected, the aim was simply to demonstrate that variation of distortion within the photographic field must be considered when calibrating large-format cameras having large radial lens distortion (i.e. nearly 700 μm) used in DR systems. Failure to do so could result in significant biases in the object space co-ordinates determined by DR. It should be pointed out that this was not of concern with the state-of-the-art solid state cameras available a decade ago (e.g., Fraser, 1997) since the image format was smaller, but is now. The hypothesis put forward here is that a better approach for cameras used in DR nowadays is to avoid the "problem" of the variation within the depth of field through aerial self-calibration in which the object distance is several orders of magnitude larger than the focal length. Figure 2 shows that for an object distance of 150 m—the lowest permissible flying height for the DR system in question over urban areas—the variation according to Brown's model is insignificant: 0.12 μm maximum. Furthermore, as will be demonstrated in the simulations, this approach can also mitigate the EO-IO correlations inherent to laboratory self-calibration.

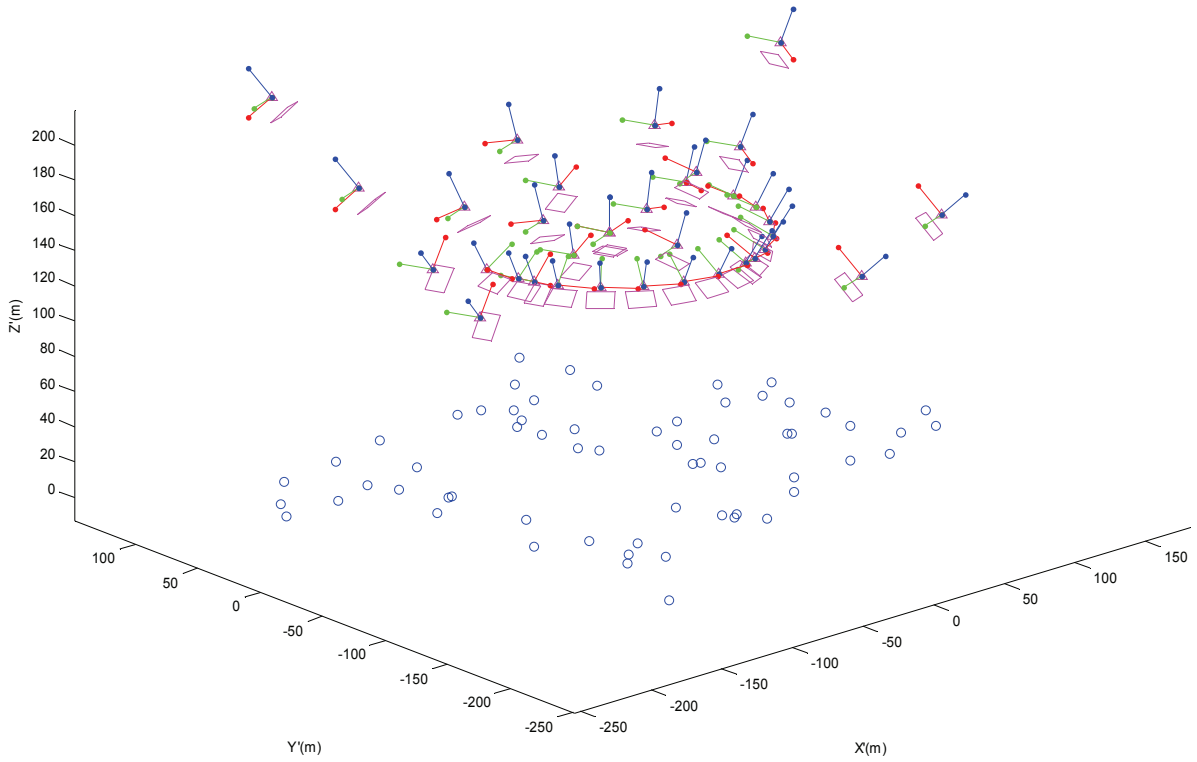

Figure 3. The simulated aerial network. Object points are denoted by the blue circles, the image space axes by the red, green and blue triad of vectors and images by the magenta rectangles.

Aerial Self-Calibration Simulations

An extensive set of realistic pre-analyses were conducted so as to optimise the aerial self-calibration network design. An urban site in Sion, Switzerland was chosen for the numerous buildings of varying height that exist there. A simulated object point field was generated from a down-sampled version of an existing DEM of the site. Comprising 59 points, the target field dimensions were 310 m x 230 m x 36 m. The flight lines were generated based on system capabilities and comprised 2 orthogonal flight lines at 150 m and a semi-circular run of images at 150 m. The maximum simulated convergence angle was 90°, which admittedly is unattainable with fix-mounted systems but theoretically possible with the hand-held design

(Skaloud et al., 2006). Two additional orthogonal flight lines at 200 m were included for two simulation cases. All images were directed toward the target field centroid so as to achieve a convergent network. The network is pictured in Figure 3.

Though many different simulations were generated, only 8 cases (A-H) are presented here. These are summarised briefly in Table 1 and some of their pertinent details are presented in Table 2 along with the relevant laboratory calibration parameters for comparison. The different observables available for the simulations include: image point co-ordinates (i); PC observations by airborne GPS; 11 independently-measured ground control points (CPs); and range measurements, ρ, between the object points and the PCs, appropriately reduced from the laser scanning system. Each case represents the addition of one or more group of observables to learn the effects on solution quality of doing so. Note that the image point precision for the aerial cases is 6 times worse than that of the lab case for which signalized targets were used but, at one-third of a pixel, is a realistic figure for an experienced operator observing distinct features. The other observation standard deviation estimates are also realistic figures derived from several years of experience in the development and use of the Scan2map/Helimap system. Note that Cases G and H are the only ones that include images at the second flying height of 200 m.

Table 1. Summary of the aerial simulation cases

Case	**Summary**
A	Free network self-calibration with only image point observations
B	Self-calibration with PC observations
C	Self-calibration with weighted ground control
D	Self-calibration with PC observations and weighted ground control
E	Self-calibration with range observations (e.g. LiDAR on board)
F	Self-calibration with PC observations, weighted ground control and range observations
G	As with Case D but with imagery at 2 flying heights
H	As with Case C but with imagery at 2 flying heights

Table 2. Pertinent details for each aerial simulation case and the laboratory calibration

	Aerial								**Lab**
	A	**B**	**C**	**D**	**E**	**F**	**G**	**H**	
σ_i (μm)	3	3	3	3	3	3	3	3	0.5
σ_{PC} (m)	-	0.03	-	0.03	-	0.03	0.03	-	-
σ_{CP} (m)	-	-	0.02	0.02	-	0.02	0.02	0.02	-
σ_ρ (m)	-	-	-	-	0.03	0.03	-	-	-
#images	15	15	15	15	15	15	23	23	16

Some of the precision and correlation results from the pre-analyses (all with minimally-constrained datum) are given in Table 3. The analysis commences with a comparison of the basic aerial case A and the laboratory calibration. Clearly the interior orientation (IO) parameters listed can be determined much more precisely in the lab than in the air primarily due to the lower image point precision of 3 μm. This advantage is, however, elusive since the PD and PC tend to vary with environmental conditions (as opposed to the radial distortion parameters) for this type of cameras (Farkas, 2007, Kremer, 2006) and therefore need to be re-determined in the air. In terms of correlation between exterior orientation (EO) and IO parameters, slight improvement is gained for the PP and PD, but the situation is worsened for

k_1. Slight de-correlation is also realised between the PD and the two radial lens distortion terms.

Table 3. Results for each aerial simulation case and the laboratory calibration

	Aerial								Lab
	A	**B**	**C**	**D**	**E**	**F**	**G**	**H**	
Precision									
σ_{xp} (μm)	1.9	1.7	1.8	1.7	1.4	1.4	1.5	1.6	0.5
σ_{yp} (μm)	2.4	2.1	2.3	2.1	1.8	1.7	1.6	1.8	0.5
σ_c (μm)	3.8	3.0	3.7	3.0	2.7	2.5	2.1	2.6	1.0
σ_{k1} x10^7	4.6	3.1	4.1	3.2	2.6	2.5	2.4	2.9	0.8
EO-IO | maximum correlation |									
PD-PC	0.66	0.45	0.51	0.31	0.37	0.28	0.25	0.48	0.84
k_1-PC	0.72	0.32	0.59	0.28	0.24	0.18	0.29	0.55	0.19
PP-angles	0.71	0.71	0.48	0.56	0.71	0.56	0.50	0.40	0.80
IO-IO Correlation									
PD-k_1	-0.13	-0.79	-0.23	-0.67	-0.72	-0.76	-0.56	-0.21	-0.33
PD-k_2	0.26	0.68	0.34	0.63	0.63	0.66	-0.54	0.31	0.39
k_1-k_2	-0.93	-0.94	-0.92	-0.93	-0.95	-0.95	-0.93	-0.92	-0.90

Addition of the PC observations (Case B) had the effect of improving the precision of the PD and k_1 and reducing the correlations between the IO and PC. However, correlation between the PD and the radial lens distortion terms was increased considerably. Clarke et al (1998) report a similar outcome for self-calibration with the PC co-ordinates fixed. The addition of a modest amount of weighted ground control (Case C) did not yield any great improvement in terms of IO precision, though all reported EO-IO correlations were reduced relative to Case A. In Case D both PC observations and the weighted CPs were added with the effect of gaining the already-mentioned benefits of both as well as the higher correlation between the PD and the lens distortion terms. In Case E only ranges from the PCs to the object points are added and the outcomes are very similar to those of Case B since they, like the airborne GPS observations, provide a priori information about the location of the PCs. All three extra observation groups were included for Case F. This produced a more favourable IO precision and EO-IO de-correlation but the correlations between the PD and lens distortion terms remain. Recognising the potential practical difficulties in correlating the laser measurements with selected image features and with the desire to lower parameter correlations further, Case G was formulated without the ranges but with the PC observations, the CPs and the images at the second flying height. Clearly this is the best aerial case in terms of IO precision. Correlation between the PD and the lens distortion terms is not as low as in the lab calibration, but this is offset by the much lower EO-IO correlation, notably between the PP and the orientation angles. Though the IO in this case is determined with lower precision, i.e. two to three times worse than the terrestrial case, this can be tolerated in light of the very favourable parameter de-correlation that is achieved. Case H comprises what can be considered the preferred geometry—a tractable number of images that achieves the desired level of de-correlation—of Case G but without the PC observations to simulate the very realistic situation where high-quality airborne GPS data may not be available due to signal interruptions. In this case IO precision is slightly worse and the IO-PC correlation coefficients are slightly higher relative to Case G, as might be expected. Interestingly, though, the latter increases are offset by reduced correlation between the PP and the angles and between the PD and the radial lens distortion terms. The correlation coefficients in this case are lower than

those from the lab calibration for the PD-PC, PP-angles and PD-lens distortion terms but not for the PC-lens distortions terms. If the high (i.e. 90°) convergence angle can not be achieved but high-quality airborne GPS observations of the PC are available, as will be seen in the real data case, all correlation coefficients remain favourable as does the IO precision except for the PD, which is degraded.

Aerial Self-Calibration: Real Data

As was anticipated, the practical realities of the data capture limited the imaging geometry and, therefore, the convergence angle that could be achieved in the network. Twenty-six images of 93 object points at the Sion site were captured with a maximum convergence angle of 60°. More object points were observed in the urban site, though only few could be used as weighted ground control. Though this and the convergence angle represented setbacks in some regards, other aspects of the solution were more favourable as explained below.

The pertinent self-calibration results are as follows. The image point residual RMS was 3.1 μm in x and 3.0 μm y. Variance component estimation indicated that these observables were optimally weighted with standard deviations of 3.5 μm, which is slightly higher than the corresponding precision estimates in the simulations. The a priori planimetric airborne GPS precision was 40 mm in X and Y and 30 mm in Z. The PC observation residual RMSs were 42 mm, 40 mm and 24 mm in X, Y and Z, respectively. Though the higher precision in Z is somewhat counter-intuitive, overall the PC precision is excellent.

Some of the outputs from the self-calibrating adjustment are presented in Table 4. The PP precision was very close to the simulated values of Case G, and the precision of k_1 was slightly better than the simulation. The PD precision was much worse, though, at ±4.3 μm. This is an expected outcome due in large part to the pointing precision of about one-third of a pixel and the lower convergence angle that were achieved. The use of structured targets and a feature-based measurement algorithm, as is done in close-range photogrammetry, could be expected to improve the precision. On the other hand, the low PD precision is not of great concern since Farkas (2007) observes its variations up to 25 μm with environmental conditions and similarly to Kremer (2006) recommends its re-adjustment on site. In case of the studied system this does not necessarily require performing aerotriangulation as the PD can be adjusted by means of the digital surface model determined simultaneously by the laser-scanner.

The real success of the in-flight calibration is the de-correlation between parameters. As can be seen from Table 4, the EO-IO correlation coefficients are very similar to those of simulation Case G. The PP-PC correlation coefficient was also analysed due to the lower convergence angle, but at 0.33 it is clearly not of concern. The most encouraging outcome is the very low correlations between the PD and the lens distortion terms, which are lower than those of both Case G and the lab self-calibration. Recalling that one of the aims from this experiment was to determine the lens distortion parameters better than in the lab, this can be regarded as a success in terms of parameter de-correlation despite the lower precision of k_1. At the maximum radial distance achieved in the laboratory (26 mm), the propagated uncertainty in the radial distortion profile is ±0.7 μm for the lab calibration and ±1.6 μm for the airborne calibration, both of which are negligible for DR.

It is important to remark here on the choice of APs. Addition of the decentring distortion parameters, p_1 and p_2—a very common practice—degrades the solution considerably due to their correlation with the PP co-ordinates (0.88 maximum correlation) and, to a lesser extent,

the orientation angles (0.67 maximum). The estimated PP precision degrades by a factor of 2 to 3.1 μm and 3.0 μm in x and y, respectively. Clearly, model identification is an important process to undertake since the choice of APs strongly dictates the estimated parameter precision.

Table 4. In-flight self-calibration results.

Precision	
σ_{xp} (μm)	1.5
σ_{yp} (μm)	1.8
σ_c (μm)	4.3
σ_{k1} x10^7	2.0
EO-IO | maximum correlation |	
PD-PC	0.34
k_1-PC	0.13
PP-angles	0.55
PP-PC	0.33
IO-IO Correlation	
PD-k_1	-0.25
PD-k_2	0.25
k_1-k_2	-0.92

Conclusions

This paper has presented an airborne approach for the geometric self-calibration of medium-format digital cameras used in direct georeferencing. This research was motivated by the problems of variation of distortion within the photographic field and high parameter correlations that can result from laboratory self-calibration. Though the exact outcomes predicted through a series of simulations were not realised due to the practical realities of system under study, the aims of the project were achieved. The primary goal of estimating the lens distortion terms was achieved in terms of their de-correlation from the other parameters while still obtaining sufficient precision. Estimation of the PP and PD was really a secondary goal as these can be re-determined by the conventional geometry of airborne AT. They are also well de-correlated but of a lower precision. The lower precision in IO is less of concern since their stability in time cannot be maintained for this type of camera and their precision is still sufficient, though an improved image point measurement procedure would allow them to be determined more precisely.

Acknowledgements

Funding for this research was provided by internal funds from EPFL and Curtin University of Technology as well as the Swiss Commission for Innovation (CTI/KTI Project 7782.1 EPRP) in collaboration with SWISSPHOTO AG. The image measurements for the airborne test were provided by Helimap SA with the supervision of Dr. Julien Vallet. The Institute of Geodesy and Photogrammetry, ETHZ provided their calibration facility and Dr. Fabio Remondino and Dr. Devrim Akca their knowledgeable assistance. These contributions are greatly appreciated.

References

Akca, D., 2006. Bundle Adjustment with Additional Parameters (BAAP), Academic software, Swiss Federal Institute of Technology Zurich (ETHZ).

Clarke, T.A., Fryer, J.G. and Wang, X., 1998. The principal point and CCD cameras. Photogrammetric Record, 16 (92): 293-312.

Brown, D.C., 1971. Close-range camera calibration. Photogrammetric Engineering, 37 (8): 855-866.

Farkas, E., 2007. Empirische Genauigkeitsuntersuchung der DigiCAM-H2/22 Luftbildkamera. Dipl.-Ing. Thesis, IFP, University of Stuttgart, 108 pp.

Fraser, C.S, 1997. Digital camera self-calibration. ISPRS Journal of Photogrammetry and Remote Sensing, 52 (4): 149-159.

Fraser, C.S. and Shortis, M.R., 1992. Variation of distortion within the photographic field. Photogrammetric Engineering and Remote Sensing, 58 (6): 851-855.

Kenefick, J., Gyer, W., and Harp, B., 1972. Analytical self-calibration. Photogrammetric Engineering, 38(11):1117 1126.

Kremer, J., 2006. System calibration of aerial camera/GPS/INS systems - procedures and experiences, International Calibration and Orientation Workshop - EuroCOW, Castelldefels, Spain, pp. 6

Kruck, E., 2001. Combined IMU and sensor calibration with BINGO-F, Integrated Sensor Orientation, Proc. of the OEEPE Workshop ". CD-ROM, Hannover, pp. 84-108

Lichti, D.D. and Chapman, M.A., 1997, Constrained FEM self-calibration, Photogrammetric Engineering and Remote Sensing, 63 (9): 1111-1119.

Mostafa, M., 2003. Design and performance of the DSS. In: D. Fritsch (Editor), Photogrammetric Week, Stuttgart

Schaer, P., 2006, Automated target extraction software utility, Swiss Federal Institute of Technology Lausanne (EPFL).

Shortis, M.R., Robson, S. and Beyer, H.A., 1998. Extended lens model calibration of digital still cameras. International Archives of Photogrammetry and Remote Sensing, 32(5): 159-164.

Skaloud, J., Vallet, J., Veyssiere, G. and Koelbl, O., 2006. An Eye for Landscape - Rapid Aerial Mapping with Handheld Sensors. GPS World(May): 7.